How many ENSO flavors can we distinguish?*

Nathaniel C. Johnson

International Pacific Research Center, SOEST, University of Hawaii at Manoa, Honolulu, Hawaii

Corresponding author address: Nathaniel Johnson, IPRC, University of Hawaii at Manoa, 401 POST Building, Honolulu, HI, 96822.
E-mail: natj@hawaii.edu

ABSTRACT

1
2

3   It is now widely recognized that the El Niño-Southern Oscillation (ENSO) occurs in

4 more than one form, with the canonical eastern Pacific (EP) and more recently recognized

5 central Pacific (CP) ENSO types receiving the most focus. Given that these various ENSO

6 "flavors" may contribute to climate variability and long-term trends in unique ways, and that

7 ENSO variability is not limited to these two types, this study presents a framework that treats

8 ENSO as a continuum but determines a finite, maximum number of statistically distinguishable

9 representative ENSO patterns. A neural network-based cluster analysis called self-organizing

10 map (SOM) analysis paired with a statistical distinguishability test determine nine unique

11 patterns that characterize the September – February tropical Pacific SST anomaly fields for the

12 period from 1950 through 2011. These nine patterns represent the flavors of ENSO, which

13 include EP, CP, and mixed ENSO patterns. Over the 1950-2011 period, the most significant

14 trends reflect changes in La Niña patterns, with a shift in dominance of La Niña-like patterns

15 with weak or negative west Pacific warm pool SST anomalies until the mid 1970s, followed by a

16 dominance of La Niña-like patterns with positive west Pacific warm pool SST anomalies,

17 particularly after the mid 1990s. Both an EP and especially a CP El Niño pattern experienced

18 positive frequency trends, but these trends are indistinguishable from natural variability.

19 Overall, changes in frequency within the ENSO continuum contributed to the pattern of tropical

20 Pacific warming, particularly in the equatorial eastern Pacific and especially in relation to

21 changes of the La Niña-like rather than El Niño-like patterns.

22

23

24

1. Introduction

The El Niño-Southern Oscillation (ENSO) is the dominant mode of tropical atmosphere-ocean interaction on interannual timescales, with impacts that span much of the globe (Ropelewski and Halpert 1987; Trenberth and Caron 2000). Typically, ENSO episodes have been identified through the monitoring of sea surface temperature (SST) anomalies in the equatorial Pacific region, most notably the so-called Niño 3.4 region (5°S - 5°N, 120 - 170°W). However, recent studies have made it increasingly clear that traditional definitions of ENSO episodes fail to distinguish two unique types of El Niño episode, the canonical El Niño that is centered in the eastern equatorial Pacific and the more recently recognized El Niño that is centered farther west near the International Date Line. This latter type, which has been referred by various names such as the "dateline El Niño" (Larkin and Harrison 2005), "El Niño Modoki" (Ashok et al. 2007), "warm pool El Niño" (Kug et al. 2009), and "central Pacific El Niño" (Yeh et al. 2009), has received increased attention because of its unique underlying dynamics (Kao and Yu 2009; Kug et al. 2009; Newman et al. 2011a,b; Yu and Kim 2011), global impacts (Larkin and Harrison 2005; Weng et al. 2007; Ashok et al. 2007; Mo 2010; Hu et al. 2012), and potential trends under global warming (Yeh et al. 2009) relative to those of the eastern Pacific (EP) El Niño. On the basis of climate model simulations analyzed in the IPCC Fourth Assessment Report, Yeh et al. (2009) suggest that the relative frequency of central Pacific (CP) El Niño episodes may increase under anthropogenic global warming in response to changes in the equatorial Pacific mean thermocline. However, the recent increasing trend in the frequency of CP El Niño episodes (Lee and McPhaden 2010) may be indistinguishable from natural variability (Newman et al. 2011b; Yeh et al. 2011).

47   The recent focus on the distinction between the EP and CP El Niño is consistent with the

48   notion that ENSO may come in many different "flavors" (Trenberth and Stepaniak 2001) that are

49   distinct from the canonical El Niño and La Niña composites and cannot be characterized by a

50   single index.   In order to describe the structure and evolution of these various flavors,

51   investigators have increasingly considered multiple indices that capture the zonal gradient of

52   equatorial Pacific SST anomalies such as the "Trans-Niño Index" (Trenberth and Stepaniak

53   2001) or, more commonly for the identification of EP and CP El Niño episodes, a comparison

54   between Niño 3 (5°S - 5°N, 150° - 90°W) and Niño 4 region (5°S - 5°N, 160°E - 150°W) SST

55   anomalies.   Although this additional information clearly reveals some of the distinct properties

56   between various ENSO episodes, such subjective index choices are not necessarily optimal for

57   describing the various ENSO flavors that are discernible in the observational record.

58   Another common approach for distinguishing tropical SST patterns is through empirical

59   orthogonal function (EOF) analysis, but this method is not guaranteed to reveal physically

60   interpretable SST modes (e.g., L'Heureux et al. 2012). In particular, the leading EOF of tropical

61   Pacific SSTs generally resembles the canonical EP ENSO pattern, and either the second (e.g.,

62   Ashok et al. 2007) or third (e.g., L'Heureux et al. 2012) EOF resembles the CP ENSO pattern.

63   However, this second or third EOF also tends to capture the spatial asymmetry between the EP

64   El Niño and La Niña patterns (Hoerling et al. 1997; Rodgers et al. 2004), which means that this

65   particular EOF is not uniquely identified with CP ENSO episodes. This complication highlights

66   one of the potential pitfalls of using a linear, orthogonal method like EOF analysis to

67   characterize nonlinear, non-orthogonal SST patterns.

68   In this study we consider a new perspective and methodology for describing ENSO

69   flavors. Under the perspective presented here, we recognize that there is a continuum of ENSO

70   states but that the relatively brief observational record limits the number of distinct ENSO

71   flavors that we can distinguish. Here we consider a methodology that treats ENSO as a

72   continuum but also determines a finite, maximum number of statistically distinguishable ENSO

73   flavors. This approach is based on a pairing of a type of neural network-based cluster analysis,

74   called self-organizing map (SOM) analysis, with a statistical distinguishability test, described

75   more thoroughly in the following section. This approach represents a more objective partitioning

76   of the equatorial Pacific SST data than the standard approach of partitioning by somewhat

77   subjective SST indices. In addition, this approach, which is constrained by neither linearity nor

78   orthogonality, avoids the disadvantages of common linear methods such as EOF analysis and

79   often results in more easily interpretable physical patterns (Reusch et al. 2005; Liu et al. 2006;

80   Johnson et al. 2008).

81   Because tropical SST trends play a critical role in remote, regional temperature and

82   precipitation trends (Shin and Sardeshmukh 2011) and tropical precipitation and circulation

83   changes (Xie et al. 2010; Johnson and Xie 2010; Ma et al. 2012; Tokinaga et al. 2012), it is

84   worthwhile to examine how changes in the frequency of different ENSO flavors impact the long-

85   term SST trend. As demonstrated and discussed in the following three sections, the framework

86   adopted here allows us to connect the long-term SST trend to changes in the frequency

87   distribution of interannually varying SST patterns.

88   The remainder of the paper is organized as follows. Section 2 provides a description of

89   the general framework, methodology, and data used in this analysis. Section 3 presents the main

90   results, which include the SOM cluster patterns and the results of the trend analysis. The paper

91   concludes with discussion and conclusions in Sections 4 and 5.

92

4

2. Data and Methodology

In this section we examine the approach for determining the ENSO region SST clusters and then determining the maximum number of distinguishable clusters.

a. Self-organizing map SST cluster patterns

Conceptually, we would expect that determining the maximum number of distinguishable ENSO flavors would require a partitioning of tropical Pacific SST fields into groups that maximize similarity within groups while also maximizing the dissimilarity between groups. Computationally, this sort of partitioning may be accomplished either by K-means cluster or SOM analysis. Specifically, K-means cluster analysis treats each SST field as an M-dimensional vector, where M is the number of grid points, and minimizes the sum of squared distances between each SST field and the nearest of the K cluster centroids. There are several reasonable choices for a distance metric, but Euclidean distance is perhaps most commonly used, and is used in the analysis presented here. The clusters are most commonly determined through an iterative, two-step procedure described as such: Given an initial assignment of K cluster centroids, which may be a random distribution, the first step is the assignment of the data vectors (SST fields in this case) to the nearest cluster centroid, and the second step is the calculation of the new cluster centroids. These two steps are repeated until the cluster assignments no longer change, which corresponds to a local minimum of the sum of squared distances described above. The value of K must be specified prior to the cluster analysis, and the method for determining K for this problem is discussed in Section 2b. K-means cluster analysis has remained a popular method of cluster analysis in the atmospheric and ocean sciences for decades (e.g., Michelangeli

116 et al. 1995; Christiansen 2007; Johnson and Feldstein 2010; Riddle et al. 2012; Freeman et al.

117 2012).

118   SOM analysis (Kohonen 2001) is a relatively new neural network-based cluster analysis

119 that bears strong similarities to K-means clustering and has increased in popularity in the

120 atmospheric and ocean sciences over the past decade (e.g., Hewitson and Crane 2002;

121 Richardson et al. 2003; Liu et al. 2006; Leloup et al. 2007; Johnson et al. 2008; Jin et al. 2010;

122 Lee et al. 2011; Chu et al. 2012). SOM analysis most significantly distinguishes itself from K-

123 means cluster analysis through the addition of a topological ordering on a low-dimensional

124 (typically one- or two-dimensional) map. In other words, the clusters "self-organize" such that

125 similar clusters are located close together on this low-dimensional map, often displayed as a grid,

126 and dissimilar clusters are located farther apart. This combination of clustering and topological

127 ordering makes SOM analysis effective for providing a visualization of the continuum of

128 patterns within a dataset. Similar to the objectives of this study, SOM analysis has been used in

129 previous studies to describe the continuum of atmospheric teleconnection patterns (e.g., Johnson

130 et al. 2008; Lee et al. 2011) and to describe decadal changes in ENSO (Leloup et al. 2007).

131   The self-organizing nature of SOM analysis owes to a component called the

132 neighborhood function, with an associated parameter called the *neighborhood radius*. When the

133 neighborhood radius is greater than zero, the clusters become organized within the low-

134 dimensional map. When the neighborhood radius is set to zero, the SOM algorithm reduces to

135 the K-means clustering algorithm. Thus, SOM analysis can be considered a "constrained version

136 of K-means clustering" (Hastie et al. 2009). In the present analysis, a one-dimensional SOM

137 analysis is performed such that the neighborhood radius gradually shrinks to a value of zero.

138 Therefore, the SOM patterns become topologically ordered along a line when the neighborhood

139   radius is greater than zero, but the algorithm used to determine the cluster patterns converges to

140   the K-means clustering algorithm. The SOM approach is chosen to ensure that similar ENSO

141   flavors are grouped together, but we would expect to see similar results with K-means cluster

142   analysis. See the appendix of Johnson et al. (2008) for a more thorough description of the basic

143   SOM methodology and Liu et al. (2006) for additional information on recommended SOM

144   parameter choices.

145   In this study, we consider ENSO flavors to be represented by SOM SST anomaly patterns

146   in the equatorial Pacific domain. We use September – February mean SST data for the period

147   from 1950 through 2011 derived from the Extended Reconstructed Sea Surface Temperature

148   Dataset, Version 3b (ERSST v3b; Xue et al. 2003; Smith et al. 2008). The September –

149   February period is used because of the seasonal phase locking of ENSO, which results in the vast

150   majority of ENSO episodes peaking during boreal fall or winter. The starting year of 1950 is

151   chosen because of the improved spatial and temporal coverage of SST data that begins around

152   that time (Deser et al. 2010; see their Fig. 3). In addition, prior to 1950 the SST patterns of

153   ENSO episodes may depend strongly on the method of reconstruction for the SST dataset (Giese

154   and Ray 2011; Ray and Giese 2012). The chosen domain covers the tropical Pacific region

155   between 120°E and 50°W and between 25°S and 25°N. The ERSST v3b data are on a 2°

156   latitude-longitude grid, but because the analysis described in the following section requires equal

157   weight to be placed on each grid point, the data are linearly interpolated to an equal-area grid

158   with 1° latitudinal spacing and longitudinal spacing that increases from 1° at the equator to

159   approximately 1.1° at 25° latitude. Anomalies are calculated by subtracting the seasonal cycle

160   for the 1981-2010 base period. The choice of the most recent 30-year climatology is based on

161   the standard practice of the National Oceanic and Atmospheric Administration (NOAA) Climate

162   Prediction Center (CPC), but the focus of this study, the spatial variations and trends of ENSO

163   flavors, is not sensitive to this choice of base period. SOM analysis is performed on the SST

164   anomaly data for various choices of K, as described in section 2b. Because the analysis

165   converges to a local rather than global minimum of the error function described at the beginning

166   of this section, the SOM analyses and all tests of Section 2b are repeated five times without any

167   noticeable change in results. Thus, the results presented here are robust. All SOM calculations

168   are performed with the Matlab SOM Toolbox (Vesanto et al. 2000) that is freely available on the

169   Web (http://www.cis.hut.fi/somtoolbox/).

170

171   *b. Determining the maximum number of distinguishable ENSO flavors*

172

173   Because K must be specified prior to a K-means cluster or SOM analysis, one challenge

174   in any cluster analysis is the determination of the optimal number of clusters. Many studies have

175   suggested various useful heuristic methods for determining K (e.g., Michelangeli et al. 1995;

176   Christiansen 2007; Hastie et al. 2009; Riddle et al. 2012), but an objective optimal K has

177   remained elusive. In this study we consider a new criterion for choosing K: the maximum

178   number such that all clusters are statistically distinguishable from another. Thus, if K^* is the

179   optimal K by this criterion, then we can determine K^* unique cluster patterns, but K^*+1 clusters

180   would result in two or more clusters that are indistinguishable by this statistical definition. In the

181   present application, K^* would refer to the maximum number of statistically discernible ENSO

182   flavors.

183   The determination of whether two cluster patterns are statistically distinguishable

184   requires a test of field significance. Often times in the atmospheric and ocean sciences, field

185   significance tests have been conducted through Monte Carlo resampling methods (Livezey and

186   Chen 1983). Recently, another field significance approach based on the "false discovery rate"

187   (FDR) has been introduced to the climate sciences (Benjamini and Hochberg 1995; Wilks 2006).

188   The FDR refers to the expected proportion of local null hypotheses that are rejected but are

189   actually true. In the present application, the local hypotheses being evaluated are whether the

190   SST anomalies at each grid point in cluster pattern i are significantly different from the

191   corresponding SST anomalies in cluster pattern j. If at least one local test has a p-value that

192   satisfies the specified FDR criterion, typically $q = 0.05$, then the cluster patterns are statistically

193   distinguishable also at the level q. If no local tests meet the FDR criterion, then the cluster

194   patterns are statistically indistinguishable. Further explanation of this test is provided below.

195   The FDR approach has a number of advantages over conventional field significance tests,

196   including generally better test power, robust results even when the local test results are correlated

197   with each other, and the identification of significant local tests while controlling the proportion

198   of false rejections (Wilks 2006). In addition, FDR tests are much more computationally efficient

199   than Monte Carlo methods, and so a large number of field significance tests can be conducted

200   with little computational effort, as required for the tests described here.

201   To determine if SOM cluster i is statistically distinguishable from SOM cluster j, we first

202   calculate the p-values (two-sided) at each grid point corresponding to the Student's t distribution

203   for a difference of means, where the null hypothesis is that the local SST composite anomalies

204   are the same in both clusters. This test is based on the recognition that SOM cluster pattern i (j)

205   with n_i (n_j) cluster members is equivalent to an SST composite pattern with n_i (n_j) samples that

9

206 comprise the composite[1]. Each of the n_i or n_j cluster members is a seasonal SST anomaly field

207 assigned to that cluster on the basis of minimum Euclidean distance. For each pair of cluster

208 pattern   composites,   we   calculate   the p-values   corresponding   to

209
$$t(\lambda,\theta) = \frac{\overline{SST_i}(\lambda,\theta) - \overline{SST_j}(\lambda,\theta)}{S(\lambda,\theta)\sqrt{\frac{1}{n_i}+\frac{1}{n_j}}},$$
(1)

210 where

211
$$S(\lambda,\theta) = \sqrt{\frac{(n_i-1)S_i(\lambda,\theta)^2 + (n_j-1)S_j(\lambda,\theta)^2}{n_i+n_j-2}}.$$
(2)

212 The variable $\overline{SST_i}$ ($\overline{SST_j}$) signifies the composite SST anomaly for SOM cluster i (j), and S_i (S_j)

213 indicates the standard deviation corresponding to all SST anomalies within cluster i (j) at latitude

214 λ and longitude θ. For these calculations, we assume that each SST anomaly field represents an

215 independent sample, which is reasonable for seasonal fields separated by at least a year and

216 usually several years within each cluster.

217   The calculations for a pair of cluster patterns described above result in a distribution of M

218 p-values, where, again, M is the total number of grid points. If all M local null hypotheses are

219 true, and if the results of the local tests are independent of each other, then the resulting M p-

220 values will be a random sample from the uniform distribution $U(0,1)$ (e.g., Folland and Anderson

221 2002; Wilks 2006). If some of the local null hypotheses are false, then the corresponding p-

222 values will be smaller than expected from this uniform distribution. The FDR test evaluates the

223 distribution of p-values to determine the local p-value that provides confidence in the correct

224 rejection of local null hypotheses; that is, the p-value that controls the FDR at the level q, which

---

[1] The equivalence between SOM cluster patterns and composites is strictly true only when the neighborhood radius of the SOM algorithm is equal to zero, as specified as the final radius in this analysis. This equivalence is always true for K-means cluster analysis.

225   is also the global or field significance level α_{global}. This test is conducted as follows. Let $p_{(m)}$

226   denote the *mth* smallest of the *M p*-values. The FDR can be controlled at the level *q* for

$$p_{FDR} = \max_{m=1,\dots,M} \left[p_{(m)} : p_{(m)} \leq q\left(\frac{m}{M}\right) \right]. \tag{3}$$

228   All local tests that yield a *p*-value less than or equal to the largest *p*-value that satisfies the right-

229   hand side of (3) are deemed significant, which means that the expected fraction of local null

230   hypotheses that are actually true for those tests is less than or equal to *q*. If no local tests meet

231   the criterion specified in (3), then the patterns are statistically indistinguishable. In the present

232   application, we shall not focus on the specific value of p_{FDR}, but instead shall focus on whether

233   or not any local tests satisfy (3) for $q = 0.05$; that is, whether or not the cluster patterns are

234   statistically distinguishable at the 95% confidence level. Although the assumption of

235   independent local tests does not hold in this case due to high spatial correlation in the SST fields,

236   the results of FDR tests do not appear sensitive to this independence assumption (Wilks 2006).

237   For *K* SOM cluster patterns there are *K*(*K*-1)/2 possible pairs of patterns to compare with

238   the test described above. To determine *K**, we perform the SOM analysis for values of *K* that

239   increase from two to 20 at an increment of one, perform the *K*(*K*-1)/2 field significance tests, as

240   described above, for each choice of *K*, and count the number of SOM cluster pattern pairs that

241   are statistically indistinguishable. The maximum number of statistically distinguishable ENSO

242   flavors, *K**, is the largest value of *K* with zero statistically indistinguishable cluster pattern pairs.

243

3. Results

245   We first examine the results of the field significance tests described above. Figure 1

246   illustrates the number of statistically indistinguishable cluster pattern pairs as a function of *K*.

247   We see that as *K* is increased from two to nine, all pairs of cluster patterns for each *K* remain

248   statistically distinguishable. When *K* is increased to ten, however, the number of statistically

249   indistinguishable pairs rises above zero. As we would expect, the number of indistinguishable

250   pairs rises monotonically with *K* above nine[2]. Thus, by the reasoning stated above, the

251   maximum number of statistically distinguishable ENSO flavors is determined to be nine.

252   The value of *K** may vary slightly based on the domain chosen to represent ENSO

253   flavors. Reasons for the slight variations include changes in the number of spatial degrees of

254   freedom, the convergence of cluster analyses to local rather than global minima of the error

255   functions, and the use of a sharp significance threshold of $\alpha_{global} = 0.05$. However, we do obtain

256   the same value of *K** when we change the northern and southern boundaries to 20°N/S or move

257   the western boundary to 90°E. Moreover, the analysis performed on both smaller and larger

258   domains results in similar interpretations of the variability and trends, supporting the robustness

259   of the results discussed below.

260

261   *a. SOM of tropical Pacific SST patterns*

262

263   With *K** determined, we now examine the nine SOM cluster patterns of tropical Pacific

264   SST anomalies. Figure 2 presents these nine patterns for the one-dimensional SOM. Because of

265   the topological ordering by the SOM, similar patterns are similarly numbered. Figure 2 reveals

266   three moderate to strong La Niña-like patterns (patterns 1-3), two weak La Niña-like patterns

267   (patterns 4-5), two weak CP El Niño-like patterns (patterns 6-7), a moderate CP/EP El Niño-like

268   pattern (pattern 8) and a strong EP El Niño-like pattern (pattern 9). In addition to amplitude, the

---

[2] If a SOM cluster has only a single member, then (1) is undefined, and the distinguishability test cannot be conducted. Therefore, in cases where a cluster only has one member, all pairs that include that particular cluster are automatically assigned as statistically indistinguishable.

269   La Niña-like patterns most significantly distinguish themselves by the longitude of maximum

270   equatorial cooling and by the presence of weak (pattern 1), negative (patterns 2 and 5), or

271   positive (patterns 3 and 4) western Pacific SST anomalies. The El Niño-like patterns also

272   distinguish themselves by amplitude and the longitude of maximum equatorial SST anomalies,

273   but the western Pacific SST anomalies are similar for each El Niño-like pattern. Pattern 9

274   resembles the canonical EP El Niño, whereas pattern 8 seemingly represents a hybrid EP/CP El

275   Niño pattern, with maximum warming in the central Pacific, but a tongue of positive SST

276   anomalies that extends to the South American coast. Together, these nine SST patterns represent

277   the ENSO SST continuum.

278   As mentioned above, each September – February SST field is assigned to the best-

279   matching SOM pattern on the basis of minimum Euclidean distance.   The frequency of

280   occurrence of each SOM pattern is indicated to the bottom right of each map, revealing that most

281   patterns occur with similar frequency. To verify that these nine patterns do, in fact, resemble the

282   seasonal SST fields that comprise the clusters, centered pattern correlations (e.g., Santer et al.

283   1993) between each SST field and its corresponding best-matching SOM pattern are calculated.

284   The mean pattern correlation is 0.76, which confirms the close resemblance between these nine

285   patterns and the individual constituent SST anomaly fields of each cluster.

286

287   *b. Changes in frequency distribution within the ENSO continuum*

288

289   Next we examine how the frequency of occurrence of these nine SOM patterns has varied

290   over the past 60 years and how these changes in frequency have influenced the long-term

291   tropical Pacific SST trends. Figure 3 illustrates the occurrence time series for each of the nine

292   patterns. This plot demonstrates that each SOM pattern generally occurs for a single season and

293   for no more than two consecutive years. In addition, Figure 3 indicates whether at least four of

294   the six months in the September through February season are classified as an El Niño or La Niña

295   episode by NOAA CPC. NOAA CPC classifies an El Niño (La Niña) episode when the three-

296   month running mean Niño 3.4 SST anomaly is greater than 0.5°C (less than -0.5°C) for at least

297   five consecutive overlapping, three-month seasons. Figure 3 confirms that patterns 1-4 are

298   closely associated with La Niña episodes, and patterns 6-9 are tied to El Niño episodes. Pattern

299   5 generally occurs when neutral ENSO conditions are declared. The CP El Niño episodes noted

300   in previous literature (e.g., Kug et al. 2009) generally correspond with SOM patterns 6 (e.g,

301   1977/78 and 1990/91), 7 (e.g., 2004/05), or 8 (e.g., 1994/95 and 2002/03). The only clearly

302   defined EP El Niño pattern, SOM pattern 9, corresponds with the strong El Niño episodes of

303   1972/73, 1982/83, and 1997/98. This observation that recent strong El Niño episodes have

304   strongly positive SST anomalies centered in the eastern Pacific, but that all other El Niño

305   episodes are centered over a broad range of longitudes is consistent with the recent studies of

306   Giese and Ray (2011) and Ray and Giese (2012).

307   Perhaps the most striking feature of Fig. 3 is the obvious trend in patterns 1-4, with

308   patterns 1 and 2 prevalent early in the period but nearly absent in the second half of the period,

309   and patterns 3 and 4 prevalent only after the mid 1990s. This trend represents a transition from

310   La Niña-like patterns with weak or negative SST anomalies in the western Pacific warm pool

311   (patterns 1 and 2) to La Niña-like patterns with positive SST anomalies in the western Pacific

312   warm pool (patterns 3 and 4).

313   This transition is demonstrated more clearly in Figure 4, which shows the trend in the

314   frequency of occurrence for each SOM pattern. Statistical significance is assessed with respect

315   to a *K*-state first-order Markov chain, as determined through a Monte Carlo test similar to that of

316   Riddle et al. (2012). For this test, 10,000 synthetic first-order Markov chain SOM pattern

317   occurrence time series (like that of Fig. 3) are generated with the same transition probabilities as

318   observed. For each synthetic time series the trend in pattern frequency of occurrence is

319   calculated. Observed trends that are greater than the 97.5[th] or less than the 2.5[th] percentile of the

320   synthetic trends are deemed statistically significant above the 95% confidence level. Figure 4

321   confirms that the trends in SOM patterns 1-4 are strongest, with only the trend in pattern 3 falling

322   just short of statistical significance. Although flavors of El Niño have received more focus than

323   those of La Niña, none of the trends in the El Niño-like patterns (patterns 6-9) is statistically

324   significant over the past 60 years.

325   To determine how these SOM pattern frequency trends have contributed to the total

326   tropical Pacific SST trends, we calculate the SOM-derived trend as

327    $$\frac{dSST_{SOM}(\lambda,\theta)}{dt} = \sum_{i=1}^{K} \frac{df_i}{dt} SST_i(\lambda, \theta),$$ (4)

328   where $\frac{df_i}{dt}$ is the frequency trend of SOM pattern *i*, and *SST$_i$* is SOM pattern *i*. Figure 5 presents

329   the total and SOM-derived September − February SST trends over the tropical Pacific region.

330   The total SST trend (Fig. 5a) reveals warming over the past 60 years over almost the entire

331   domain, but the most pronounced warming is indicated over the eastern equatorial Pacific and

332   western Pacific warm pool. The trend derived from (4) (Fig. 5b) also shows warming over most

333   of the domain, but the warming is most pronounced only over the eastern Pacific region. Figure

334   4 suggests that most of these ENSO flavor-related trends relate to changes in the frequency of La

335   Niña-like rather than El Niño-like patterns. This suggestion is confirmed in Fig. 6, which shows

336   the trends from the application of (4) only for La Niña-like SOM patterns 1-5 (Fig. 6a) and only

337   for El Niño-like SOM patterns 6-9 (Fig. 6b). The trend pattern derived solely from La Niña-like

15

338   pattern frequency changes (Fig. 6a) closely resembles the total ENSO-related trend pattern (Fig.

339   5b). The positive trends in El Niño-like pattern frequencies have contributed to modest warming

340   in the eastern equatorial Pacific region, but El Niño-related trends are weak throughout the rest

341   of the domain (Fig. 6b).

342   The difference between the total and SOM-derived trends (Fig. 5c) reveals generally

343   weak and even negative SST trends over the equatorial Pacific domain but with pronounced

344   positive trends remaining over the west Pacific warm pool. This result suggests that trends in the

345   frequency of occurrence of various ENSO flavors have dominated the SST trends in the eastern

346   equatorial Pacific region, but the trends in the west Pacific warm pool reflect a combination of

347   changes in frequency distribution and an additional superimposed long-term non-ENSO trend.

348

349   4. Discussion

350   The preceding analysis reveals nine statistically distinguishable patterns that represent the

351   ENSO continuum. This continuum perspective contrasts the framework of recent studies that

352   suggest two clearly distinct types of El Niño. This continuum perspective also is supported by

353   the recent work of Giese and Ray (2011), who find that the central longitude of El Niño SST

354   anomalies is not bimodal but rather is indistinguishable from a Gaussian distribution centered

355   near 140°W. One notable observation is that the three strongest El Niño episodes of the past 60

356   years as measured by Niño 3.4 SST anomalies (1972/73, 1982/83, and 1997/98) feature strongest

357   SST anomalies in the eastern Pacific (SOM pattern 9). Perhaps the increased attention paid to

358   these strongest episodes has resulted in an over-emphasized sharpening of the differences

359   between EP and CP El Niño episodes. Evidence from an ocean reanalysis suggests that these

360   strong EP El Niño episodes may have resulted in an eastward bias of reconstructed El Niño SST

16

361 anomalies for periods before 1950 owing to the influence of these strong El Niño episodes on the

362 SST reconstructions (Giese and Ray 2011; Ray and Giese 2012).

363 The analysis also reveals that these nine ENSO flavors have made a significant

364 contribution to the long-term tropical Pacific SST trend through changes in their frequency

365 distribution (Fig. 5b). The most significant trends relate to the La Niña-like patterns, with the

366 dominance of patterns with negative western Pacific SST anomalies (patterns 1 and 2) before the

367 mid 1970s followed by the dominance of patterns with positive western Pacific SST anomalies

368 (patterns 3 and 4) after the mid 1970s, particularly from the mid 1990s to the present. These

369 frequency trends have contributed to tropical Pacific warming, particularly in the western Pacific

370 and eastern equatorial Pacific regions (Fig. 6a). One may hypothesize that this behavior reflects

371 a long-term warming trend most pronounced in the western Pacific warm pool superimposed on

372 interannual ENSO variability. However, this analysis suggests that there is a disproportionate

373 western Pacific warming for La Niña-like patterns, while there is no similar trend in the western

374 Pacific evident for the El Niño-like patterns[3]. In fact, the positive trend in the frequency of El

375 Niño-like patterns, particularly pattern 8, contributes to a weak *negative* SST trend in the west

376 Pacific warm pool region (Fig. 6b). Therefore, this analysis suggests that the simple paradigm of

377 a long-term trend superimposed on interannual variability, as typically assumed in global

378 warming attribution studies (e.g., Pall et al. 2011), may not be sufficient for understanding

379 tropical Pacific SST variability and trends. Rather, changes in the frequency distribution of

380 interannually varying patterns within the ENSO continuum, as depicted in Fig. 2, may impart a

381 significant contribution to the long-term trend. Moreover, recent theoretical work (Liang et al.

382 2012) proposes that the recent elevation in ENSO variance may be more of a cause than a

---

[3] See Fig. 10 of L'Heureux et al. (2012) for additional evidence of enhanced west Pacific warm pool warming trends in La Niña episodes relative to El Niño episodes during November – February.

17

383　consequence of eastern tropical Pacific warming, which would further underscore the difficulty

384　of separating interannual variability from the tropical mean state.

385　　　　The trend toward La Niña-like patterns with positive SST anomalies in the western

386　Pacific warm pool is of particular interest because this general pattern may represent the "perfect

387　ocean for drought" over many midlatitude regions (Hoerling and Kumar 2003). This SST

388　pattern, captured by SOM patterns 3 and 4, dominated during the period between 1998 and 2002

389　(Fig. 3), which was a period of prolonged drought throughout much of the United States,

390　southern Europe, and Southwest Asia. Climate model simulations suggest that both the negative

391　SST anomalies in the eastern Pacific and positive SST anomalies in the western tropical Pacific

392　acted synergistically to force the persistent drought during this period (Hoerling and Kumar

393　2003; Lau et al. 2006). Figure 3 reveals that SOM patterns 3 and 4 occurred several additional

394　times since that period. In addition, there is evidence that the positive trend in Indo-Pacific

395　warm pool SSTs has contributed to changes in the wintertime teleconnection response to La

396　Niña, a trend toward a more zonally oriented circumglobal teleconnection pattern (Kumar et al.

397　2010; Lee et al. 2011). Given the widespread societal impacts of these particular La Niña

398　flavors, it is worthwhile for future studies to investigate whether the disproportionate warm pool

399　warming for La Niña-like patterns shall continue.

400　　　　Both an EP (pattern 9) and CP/EP El Niño (pattern 8) SOM pattern also have experienced

401　positive trends in the frequency of occurrence over the past 60 years, but these trends are

402　indistinguishable from natural variability (Fig. 4). Given the recent focus on whether CP El

403　Niño episodes will become more frequent under global warming (Yeh et al. 2009), the positive

404　trend of CP El Niño-like SOM pattern 8 is of particular interest. However, the lack of a

405　significant trend is consistent with recent studies based on long integrations of a multivariate red

406   noise model (Newman et al. 2011b) and a coupled climate model (Yeh et al. 2011), which found

407   that the recent multidecadal increase in CP El Niño relative to EP El Niño episodes is consistent

408   with natural variability.

409   The changes in frequency of the ENSO flavor SOM patterns have contributed to an

410   overall positive SST trend in the central and eastern equatorial Pacific region (Fig. 5b), which is

411   consistent with recent findings linking positive equatorial Pacific trends to ENSO (Compo and

412   Sardeshmukh 2010; Lee and McPhaden 2010; L'Heureux et al. 2012). In addition, the increased

413   dominance of SOM patterns 3 and 4 at the expense of patterns 1 and 2 has contributed to the

414   warming trend in the tropical West Pacific region. The residual SST trend (Fig. 5c) reveals

415   positive SST trends in the western Pacific but weak or even negative SST trends throughout the

416   equatorial eastern Pacific region. Interestingly, this residual trend in Fig. 5c is somewhat similar

417   to the ENSO-unrelated SST trends obtained after applying a dynamic ENSO filter (Compo and

418   Sardeshmukh 2010; Solomon and Newman 2012). This particular filter, which accounts for the

419   SST evolution during ENSO and is obtained through a linear inverse modeling approach, reveals

420   a trend pattern of western Indo-Pacific warming and eastern equatorial Pacific cooling after the

421   trends associated with ENSO have been removed. The approach adopted here similarly shows

422   that ENSO-related trends have contributed to eastern equatorial Pacific warming (Fig. 5b), and

423   the residual SST warming is most pronounced in the west Pacific warm pool (Fig. 5c).

424   However, we must exercise caution when viewing long-term SST trends, given the data

425   uncertainties. In particular, a recent SST reconstruction based only on bucket SST and nighttime

426   marine surface air temperature measurements suggests less pronounced western Pacific warming

427   relative to that of the eastern Pacific (Tokinaga et al. 2012). Although beyond the scope of this

428   study, future research shall continue to investigate whether this enhanced western Pacific

19

429   warming is real, and, if so, whether it represents a response to anthropogenic warming (Clement

430   et al. 1996, Cane et al. 1997) or if enhanced equatorial Pacific warming, as in global climate

431   models (Collins et al. 2010; Xie et al. 2010), is more likely. The interplay between the potential

432   impact of greenhouse gas warming on ENSO (Guilyardi et al. 2009; Yeh et al. 2009; Collins et

433   al. 2010; Vecchi and Wittenberg 2010) and on long-term SST trends is a challenging problem,

434   but the approach presented here provides a possible framework for exploring this interaction.

435

436   5. Conclusions

437   This study opens with the question: how many ENSO flavors can we distinguish? To

438   address this question, we examine an approach that partitions tropical Pacific SST fields through

439   SOM analysis and then determines the maximum number of SOM cluster patterns that are

440   statistically distinguishable. This approach can be applied more generally to other cluster

441   analysis problems, particularly those of K-means cluster or SOM analysis, in order to answer the

442   recurring question of what is the optimal, or at least the maximum number of clusters to retain.

443   The approach adopted here has the appeal of being grounded in an accessible concept, statistical

444   distinguishability. Many other applications with serially correlated data would face the

445   additional challenge of accounting for serial correlation in the calculation of local p-values, but

446   the basic approach described here still would apply.

447   Although the present study focuses on seasonal SST patterns, ENSO also undergoes other

448   types of interdecadal variations, including changes in the seasonal evolution of ENSO-related

449   SST anomalies. Future extensions of this study may explore seasonal variations of ENSO

450   flavors. In addition, the dynamical processes responsible for these nine patterns remain an open

451   question. Through a multivariate red noise framework for tropical SST variability, Newman et

452   al. (2011a,b) find that the leading optimal structure corresponding with the EP ENSO is driven

453   by both surface and thermocline interactions, as in the classic "recharge-discharge" mechanism

454   (Jin 1997). In contrast, the optimal structure corresponding with CP ENSO evolves through non-

455   local SST interactions, such as the advection of SST anomalies, but without the recharge-

456   discharge mechanism. The CP ENSO event growth is more modest than that of the EP ENSO,

457   but the lack of a discharge mechanism allows the CP ENSO to decay more slowly (Newman et

458   al. 2011b). Because these two optimal initial structures are orthogonal, the framework of

459   Newman et al. (2011a,b) suggests a continuum of "mixed" CP/EP ENSO patterns with

460   intermediate dynamical characteristics. The analysis presented here is consistent with this

461   general framework, but additional work is needed.

462   The analysis presented here also suggests that although El Niño flavors often receive

463   more focus than those of La Niña in the literature, changes related to La Niña-like SST patterns

464   have made a stronger impact on long-term SST trends over the past 60 years. A number of

465   outstanding questions remain. Given that tropical Pacific SST anomalies have far-reaching

466   effects through tropical convection anomalies and the triggering of atmospheric teleconnections,

467   future research shall augment recent efforts (e.g., Larkin and Harrison 2005; Weng et al. 2007;

468   Mo 2010; Hu et al. 2012) to examine how many ENSO flavor teleconnections and remote

469   impacts can be distinguished. In addition, the various ENSO flavors within the ENSO

470   continuum and their relationship with the long-term SST trend remain an active area of research

471   (Guilyardi et al. 2009; Yeh et al. 2009; Collins et al. 2010; Liang et al. 2012). A unique set of

472   questions raised in this study relates to the trend toward La Niña-like patterns with enhanced

473   SST anomalies in the west Pacific warm pool. Why has there been disproportionate west Pacific

474   warming for La Niña patterns? Will this trend continue? Can coupled global climate models

475   capture this sort of variability? The approach presented here provides a framework for

476   examining the ENSO continuum and questions like these with a manageable set of representative

477   ENSO flavors.

478

486

487

References

489   Ashok, K., S. K. Behera, S. A. Rao, H. Weng, and T. Yamagata, 2007: El Niño Modoki and its

490   possible teleconnection. *J. Geophys. Res.*, **112**, C11007, doi:10.1029/2006JC003798.

491

492   Benjamini, Y., and Y. Hochberg, 1995: Controlling the false discovery rate: A practical and

493   powerful approach to multiple testing. *J. Roy. Stat. Soc.*, **B57**, 289-300.

494

495   Cane, M. A., A. C. Clement, A. Kaplan, Y. Kushnir, D. Pozdnyakov, R. Seager, S. E. Zebiak,

496   and R. Murtugudde, 1997: Twentieth-century sea surface temperature trends. *Science*, **275**, 957-

497   960.

498

499   Christiansen, B., 2007: Atmospheric circulation regimes: Can cluster analysis provide the

500   number?. *J. Climate*, **20**, 2229–2250.

501

502   Chu, J.-E., S. N Hameed, and K.-J. Ha, 2012: Non-linear, intraseasonal phases of the East Asian

503   summer monsoon: Extraction and analysis using self-organizing maps. *J. Climate*, in press.

504

505   Collins, M., S.-I An, W. Cai, A. Ganachaud, E. Guilyardi, F.-F. Jin, M. Jochum, M. Lengaigne,

506   S. Power, A. Timmermann, G. Vecchi, and A. Wittenberg, 2010: The impact of global warming

507   on the tropical Pacific Ocean and El Niño. *Nat. Geosci.*, **3**, 391-397.

508

509   Compo, G. P., and P. D. Sardeshmukh, 2010: Removing ENSO-Related variations from the

510   climate record. *J. Climate*, **23**, 1957–1978.

511

512   Deser, C., M. A. Alexander, S.-P. Xie, and A. S. Phillips, 2010: Sea surface temperature

513   variability: patterns and mechanisms. *Ann. Rev. Mar. Sci.*, **2010.2**, 115-143.

514

515   Folland, C., C. Anderson, 2002: Estimating changing extremes using empirical ranking methods.

516   *J. Climate*, **15**, 2954–2960.

517

518   Freeman, L. A., A. J. Miller, R. D. Norris, and J. E. Smith, 2012: Classification of remote Pacific

519   coral reefs by physical oceanographic environment, *J. Geophys. Res.*, **117**, C02007,

520   doi:10.1029/2011JC007099.

521

522 Giese, B. S., and S. Ray, 2011: El Niño variability in simple ocean data assimilation (SODA),

523 1871-2008. *J. Geophys. Res.*, **116**, C02024, doi:10.1029/2010JC006695.

524

525 Guilyardi, E., A. Wittenberg, A. Fedorov, M. Collins, C. Wang, A. Capotondi, G. J. van

526 Oldenborgh, T. Stockdale, 2009: Understanding El Niño in ocean–atmosphere general

527 circulation models: Progress and challenges. *Bull. Amer. Meteor. Soc.*, **90**, 325–340.

528

529 Hastie, T., R. Tibshirani, and J. Friedman, 2009: Unsupervised learning. *The Elements of*

530 *Statistical Learning: Data Mining, Inference, and Prediction*, Springer, 485-585.

531

532 Hewitson, B.C., and R. G. Crane, 2002: Self-organizing maps: Applications to synoptic

533 climatology. *Clim. Res*., **22**, 13-26.

534

535 Hoerling, M. P., and A. Kumar, 2003: The perfect ocean for drought. *Science*, **299**, 691-694.

536

537 Hoerling, M. P., A. Kumar, and M. Zhong, 1997: El Niño, La Niña, and the nonlinearity of their

538 teleconnections. *J. Climate*, **10**, 1769–1786.

539

540 Hu, Z.-Z., A. Kumar, B. Jha, W. Wang, B. Huang, and B. Huang, 2012: An analysis of warm

541 pool and cold tongue El Niños: air-sea coupling processes, global influences, and recent trends.

542 *Climate Dyn.*, in press, doi:10.1007/s00382-011-1224-9.

543

544   Jin, B., G. Wang, Y. Liu, and R. Zhang, 2010: Interaction between the East China Sea Kuroshio

545   and the Ryukyu Current as revealed by the self-organizing map, *J. Geophys. Res.*, **115**, C12047,

546   doi:10.1029/2010JC006437.

547

548   Jin, F.-F., 1997: An equatorial ocean recharge paradigm for ENSO. Part I: Conceptual model. *J.*

549   *Atmos. Sci.*, **54**, 811-829.

550

551   Johnson, N. C., and S. B. Feldstein, 2010: The continuum of North Pacific sea level pressure

552   patterns: Intraseasonal, interannual, and interdecadal variability. *J. Climate*, **23**, 851–867.

553

554   Johnson, N. C., S. B. Feldstein, and B. Tremblay, 2008: The continuum of Northern Hemisphere

555   teleconnection patterns and a description of the NAO Shift with the use of self-organizing maps.

556   *J. Climate*, **21**, 6354–6371.

557

558   Johnson, N. C., and S.-P. Xie, 2010: Changes in the sea surface temperature threshold for

559   tropical convection. *Nat. Geosci.*, **3**, 842-845.

560

561   Larkin, N. K, and D. E. Harrison, 2005: Global seasonal temperature and precipitation anomalies

562   during El Niño. *Geophys. Res. Lett.*, **32**, L16705, doi:10.1029/2005GL022860.

563

564   Leloup, J., Z. Lachkar, J.-P. Boulanger, and S. Thiria, 2007: Detecting decadal changes in ENSO

565   using neural networks. *Climate Dyn.*, **28**, 147-162, doi:10.1007/s00382-006-0173-1.

566

567   Kao, H.-Y., and J.-Y. Yu, 2009: Contrasting eastern-Pacific and central-Pacific types of ENSO.

568   *J. Climate*, **22**, 615-632.

569

570   Kohonen, T., 2001: *Self-Organizing Maps*. Springer, 501.

571

572   Kug, J.-S., F.-.F. Jin, and S.-I. An, 2009: Two types of El Niño events: Cold tongue El Niño and

573   warm pool El Niño. *J. Climate*, **22**, 1499-1515.

574

575   Kumar, A., B. Jha, and M. L'Heureux, 2010: Are tropical SST trends changing the global

576   teleconnection during La Niña? *Geophys. Res. Lett.*, **37**, L12702, doi:10.1029:2010GL043394.

577

578   Lau, N.-C., A. Leetmaa, M. J. Nath, and H.-L. Wang, 2006: Attribution of atmospheric

579   variations in the 1997-2003 period to SST anomalies in the Pacific and Indian Ocean basins. *J.*

580   *Climate*, **19**, 3607-3628.

581

582   Lee, S., T. Gong, N. Johnson, S. B. Feldstein, and D. Pollard, 2011: On the possible link between

583   tropical convection and the Northern Hemisphere Arctic surface air temperature change between

584   1958 and 2001. *J. Climate*, **24**, 4350–4367.

585

586   Lee, T., and M. J. McPhaden, 2010: Increasing intensity of El Niño in the central-equatorial

587   Pacific. *Geophys. Res. Lett.*, **37**, L14603, doi:10.1029/2010GL044007.

588

589   L'Heureux, M. L., D. C. Collins, and Z.-Z. Hu, 2012: Linear trends in sea surface temperature of

590   the tropical Pacific Ocean and implications for the El Niño-Southern Oscillation. *Climate Dyn.*,

591   in press, doi:10.1007/s00382-012-1331-2.

592

593   Liang, J., X.-Q. Yang, and D.-Z. Sun, 2012: The effect of ENSO events on the tropical Pacific

594   mean climate: Insights from an analytical model. *J. Climate*, **25**, 7590-7606.

595

596   Liu, Y., R. H. Weisberg, and C. N. K. Mooers, 2006: Performance evaluation of the self-

597   organizing   map   for   feature   extraction. *J.   Geophys.   Res.*, **111**,   C05018,

598   doi:10.1029/2011GL047658.

599

600   Livezey, R. E., and W. Y. Chen, 1983: Statistical field significance and its determination by

601   Monte Carlo techniques. *Mon. Wea. Rev*., **111**, 46-59.

602

603   Ma, J., S.-P. Xie, and Y. Kosaka, 2012: Mechanisms for tropical tropospheric circulation change

604   in response to global warming. *J. Climate*, **25**, 2979-2993.

605

606   Michelangeli, P.-A., R. Vautard, and B. Legras, 1995: Weather regimes: Recurrence and quasi

607   stationarity. *J. Atmos. Sci.*, **52**, 1237–1256.

608

609   Newman M., M. A. Alexander, and J. D. Scott, 2011a: An empirical model of tropical ocean

610   dynamics. *Climate Dyn.*, **37**, 1823-1841.

611

612 Newman, M., S.-I. Shin, and M. A. Alexander, 2011b: Natural variation in ENSO flavors.

613 *Geophys. Res. Lett.*, **38**, L14705, doi:10.1029/2011GL047658.

614

615 Pall, P., T. Aina, D. A. Stone, P. A. Stott, T. Nozawa, A. G. J. Hilberts, D. Lohmann, and M. R.

616 Allen, 2011: Anthropogenic greenhouse gas contribution to flood risk in England and Wales in

617 autumn 2000. *Nature*, **470**, 382-385.

618

619 Ray, S., and B. S. Giese, 2012: Historical changes in El Niño and La Niña characteristics in an

620 ocean reanalysis. *J. Geophys. Res.*, **117**, C11007, doi:10.1029/2012JC008031.

621

622 Riddle E. E., M. B. Stoner, N. C. Johnson, M. L. L'Heureux, D. C. Collins, and S. B. Feldstein,

623 2012: The impact of the MJO on clusters of wintertime circulation anomalies over the North

624 American region. *Climate Dyn.,* in press, doi:10.1007/s00382-012-1493-y.

625

626 Rodgers, K. B., P. Friederichs, and M. Latif, 2004: Tropical Pacific decadal variability and its

627 relation to decadal modulation of ENSO. *J. Climate*, **17**, 3761-3774.

628

629 Reusch, D. B., R. B. Alley, and B. C. Hewitson, 2005: Relative performance of self-organizing

630 maps and principal component analysis in pattern extraction from synthetic climatological data.

631 *Polar Geogr.*, **29**, 227-251.

632

633 Richardson, A. J., C. Risien, and F. A. Shillington, 2003: Using self-organizing maps to identify

634 patterns in satellite imagery. *Prog. Oceanog.*, **59**, 223-239.

635

636 Ropelewski, C. F., M. S. Halpert, 1987: Global and regional scale precipitation patterns

637 associated with the El Niño/Southern Oscillation. *Mon. Wea. Rev.*, **115**, 1606–1626.

638

639 Santer, B. D., T. M. L. Wigley, and P. D. Jones, 1993: Correlation methods in fingerprint

640 detection studies. *Climate Dyn.*, **8**, 265-276.

641

642 Shin, S.-I., and P. D. Sardeshmukh, 2011: Critical influence of the pattern of tropical ocean

643 warming on remote climate trends. *Climate Dyn.*, **36**, 1577-1591.

644

645 Smith, T.M., R.W. Reynolds, T. C. Peterson, and J. Lawrimore, 2008: Improvements to NOAA's

646 Historical Merged Land-Ocean Surface Temperature Analysis (1880-2006). *J. Climate*, **21**,

647 2283-2296.

648

649 Solomon, A., and M. Newman, 2012: Reconciling disparate twentieth-century Indo-Pacific

650 ocean temperature trends in the instrumental record. *Nature Climate Change*,

651 doi:10.1038/NCLIMATE1591.

652

653 Tokinaga, H., S.-P. Xie, C. Deser, Y. Kosaka, and Y. M. Okumura, 2012: Slowdown of the

654 Walker circulation driven by tropical Indo-Pacific warming. *Nature*, **491**, 439-443.

655

656 Trenberth, K. E., and J. M. Caron, 2000: The Southern Oscillation revisited: sea level pressures,

657 surface temperatures, and precipitation. *J. Climate*, **13**, 4358-4365.

658

659 Trenberth, K. E., and D. P. Stepaniak, 2001: Indices of El Niño. *J. Climate*, **14**, 1697-1701.

660

661 Vecchi, G.A. and A.T. Wittenberg, 2010: El Niño and our future climate: where do we stand?

662 *WIREs Clim. Change*, **1**, 260-270.

663

664 Vesanto, J., J. Himberg, E. Alhoniemi, and J. Parhankangas, 2000: SOM toolbox for Matlab 5.

665 Helsinki University of Technology, Finland. [Available online at

666 http://www.cis.hut.fi/projects/somtoolbox/.]

667

668 Weng, H., K. Ashok, S. K. Behera, S. A. Rao, and T. Yamagata, 2007: Impacts of recent El Niño

669 Modoki on dry/wet conditions in the Pacific Rim during boreal summer. *Climate Dyn.*, **29**, 113-

670 129.

671

672 Xie, S.-P., C. Deser, G. A. Vecchi, J. Ma, H. Teng, and A. T. Wittenberg, 2010: Global warming

673 pattern formation: Sea surface temperature and rainfall. *J. Climate*, **23**, 966–986.

674

675 Xue, Y., T. M. Smith, and R. W. Reynolds, 2003: Interdecadal changes of 30-yr SST normals

676 during 1871-2000. *J. Climate*, **16**, 1601-1612.

677

678 Yeh, S.-W, B. K. Kirtman, J.-S. Kug, W. Park, and M. Latif, 2011: Natural variability of the

679 central Pacific El Niño event on multi-centennial timescales. *Geophys. Res. Lett.*, **38**, L02704,

680 doi:10.1029/2010GL045886.

681

682   Yeh, S.-W., J.-S. Kug, B. Dewitte, M.-H. Kwon, B. P. Kirtman, and F.-F. Jin, 2009: El Niño in a

683   changing climate. *Nature*, **461**, 511-514.

684

685   Yu, J.-Y., and S. T. Kim, 2011: Relationships between extratropical sea level pressure variations

686   and the central Pacific and eastern Pacific types of ENSO. *J. Climate*, **24**, 708-720.

687

688   Wilks, D. S., 2006: On "field significance" and the false discovery rate. *J. Appl. Meteor.*

689   *Climatol.*, **45**, 1181-1189.

690

691

692

693

694

695

696

697

698

699

700

701

702

703

704

31

List of Figures

728   FIG. 6. As in Fig. 5b but calculated only for (a) La Niña-like SOM patterns 1-5 and for (b) El

729   Niño-like SOM patterns 6-9.

730

731

732

733

734

735

736

737

738

739

740
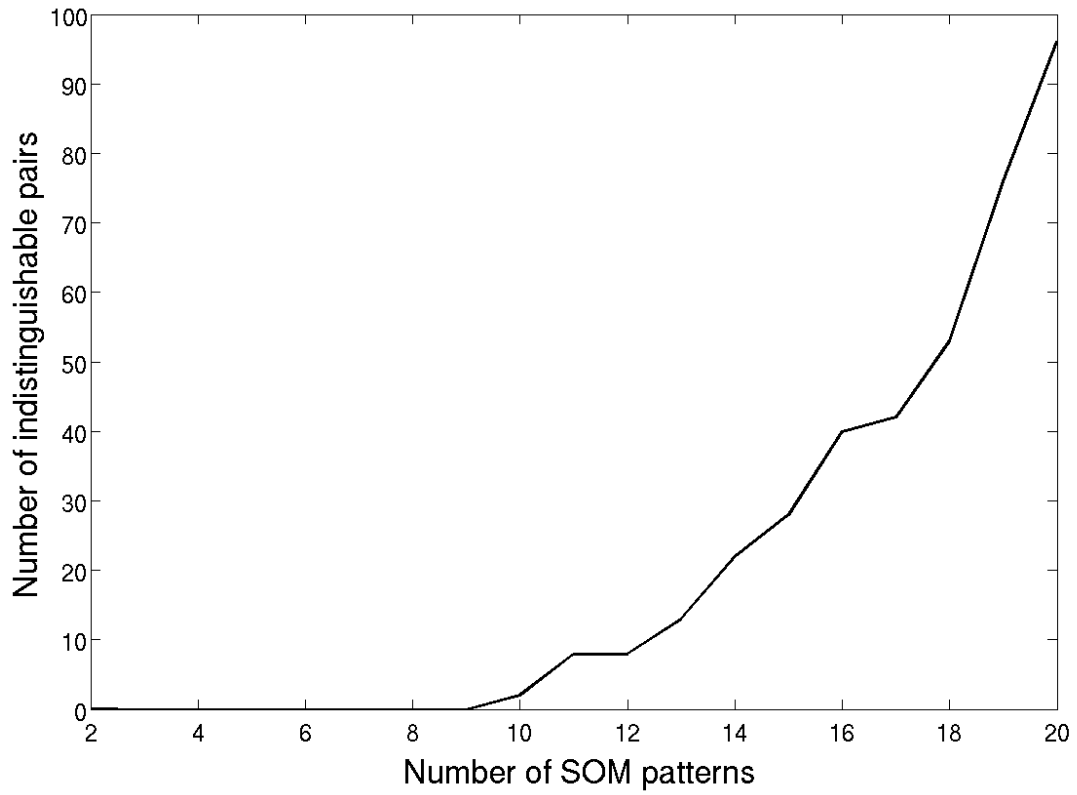
FIG. 1. The number of SOM SST cluster pattern pairs that are statistically indistinguishable at the

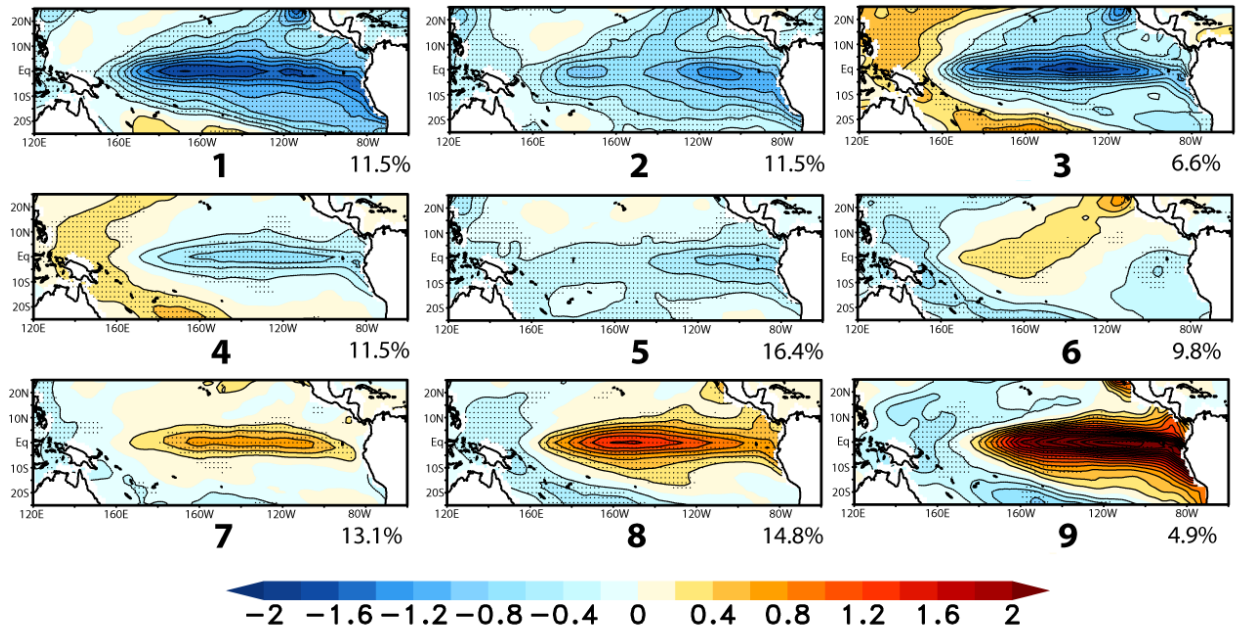95% confidence level as a function of the number of SOM patterns, *K*.

FIG. 2. The nine SST anomaly cluster patterns for a one-dimensional SOM. The contour interval is 0.2°C, with the zero contour line omitted. Stippling indicates anomalies that are statistically significant above the 95% confidence level. The percentages to the bottom right of each map refer to the frequency of occurrence of the pattern for the 1950-2011 period.
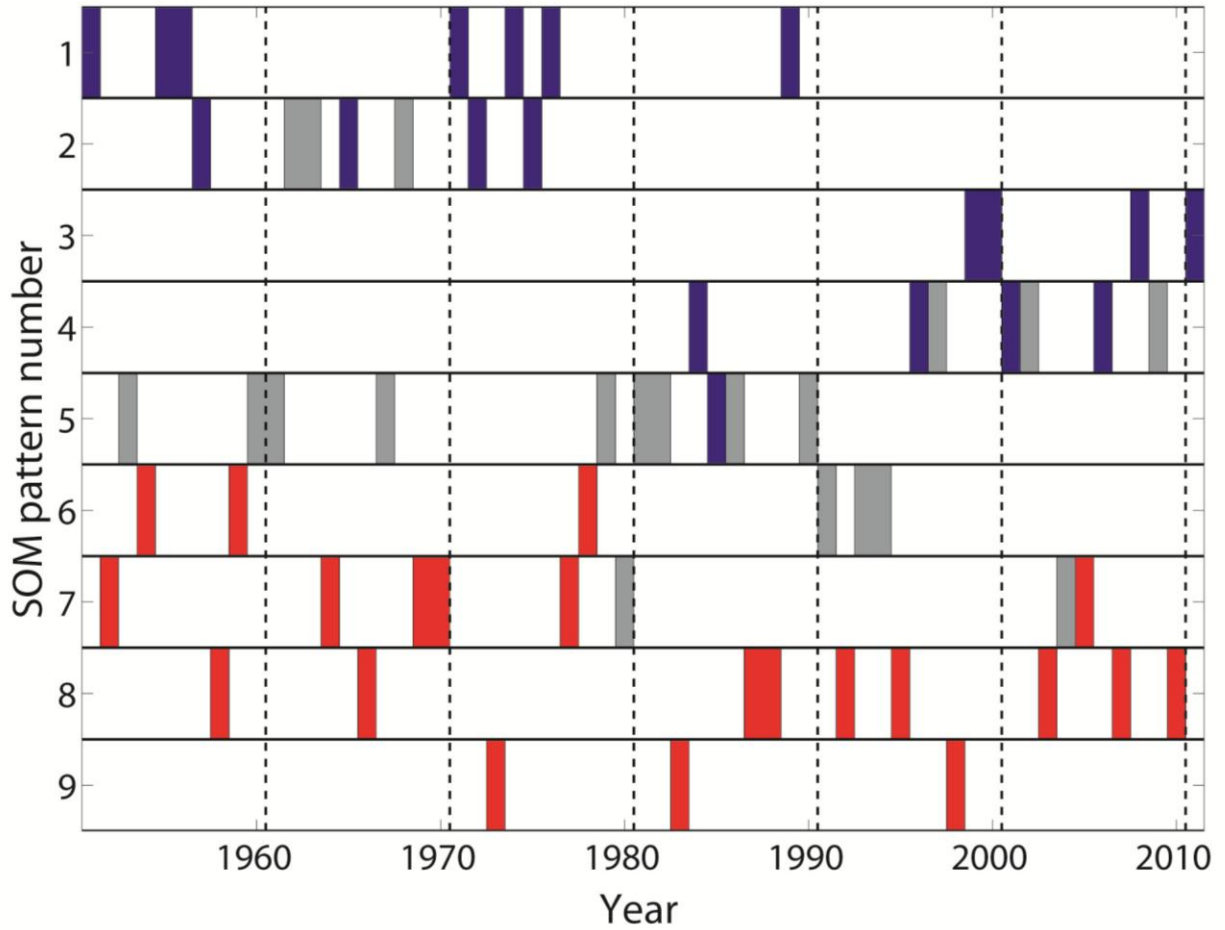
FIG. 3. Occurrence time series for each of the nine SOM patterns in Figure 2 (the assigned year corresponds to that of January-February in the September-February season). Filled bars indicate pattern occurrence for the particular year. Red (blue) bars indicate the occurrence of an El Niño (La Niña) episode during at least four of the six months, and grey bars indicate the classification as an ENSO neutral season.
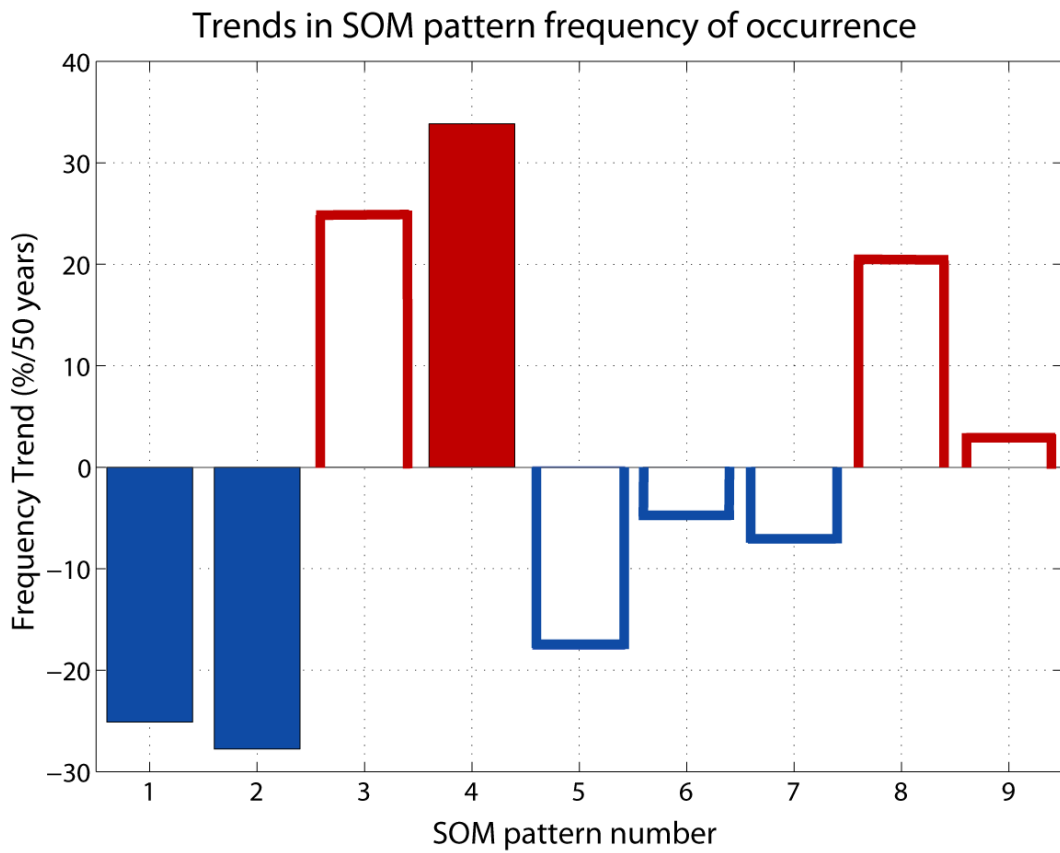
36

FIG. 4. Trends in the frequency of occurrence for each of nine SOM patterns in Figure 2. Filled bars signify trends that are statistically significant above the 95% confidence level with respect to a nine-state first-order Markov chain (see text for details).
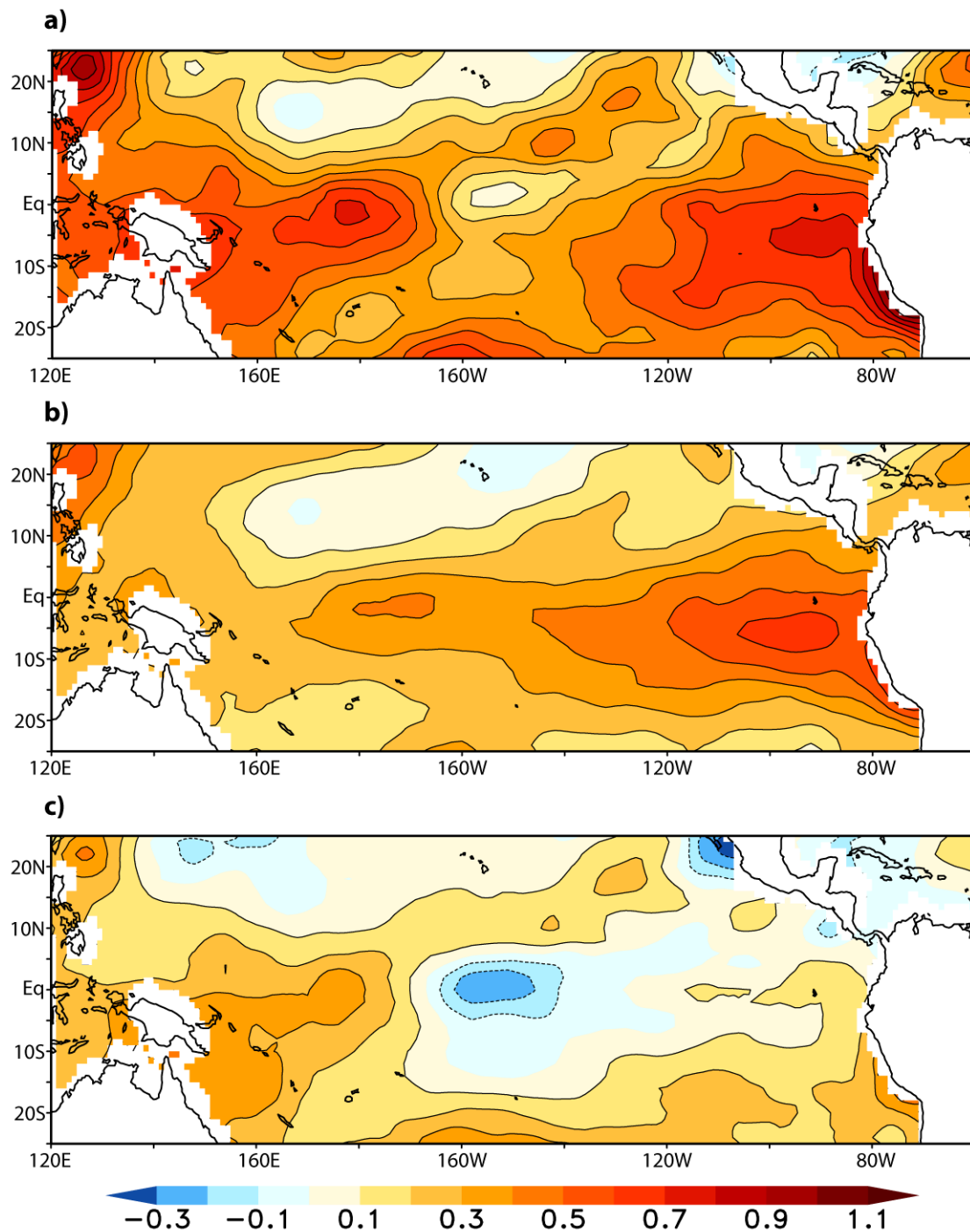
FIG. 5. (a) Total and (b) SOM-derived September – February SST trend (°C/50 years) for 1950-2011. (c) Difference between total and SOM-derived SST trends [(a) minus (b)]. The contour interval is 0.1°C/50 years, and the zero contour line is omitted.

38

a) SST Trend Attributed to La Nina-like patterns (SOM patterns 1-5)

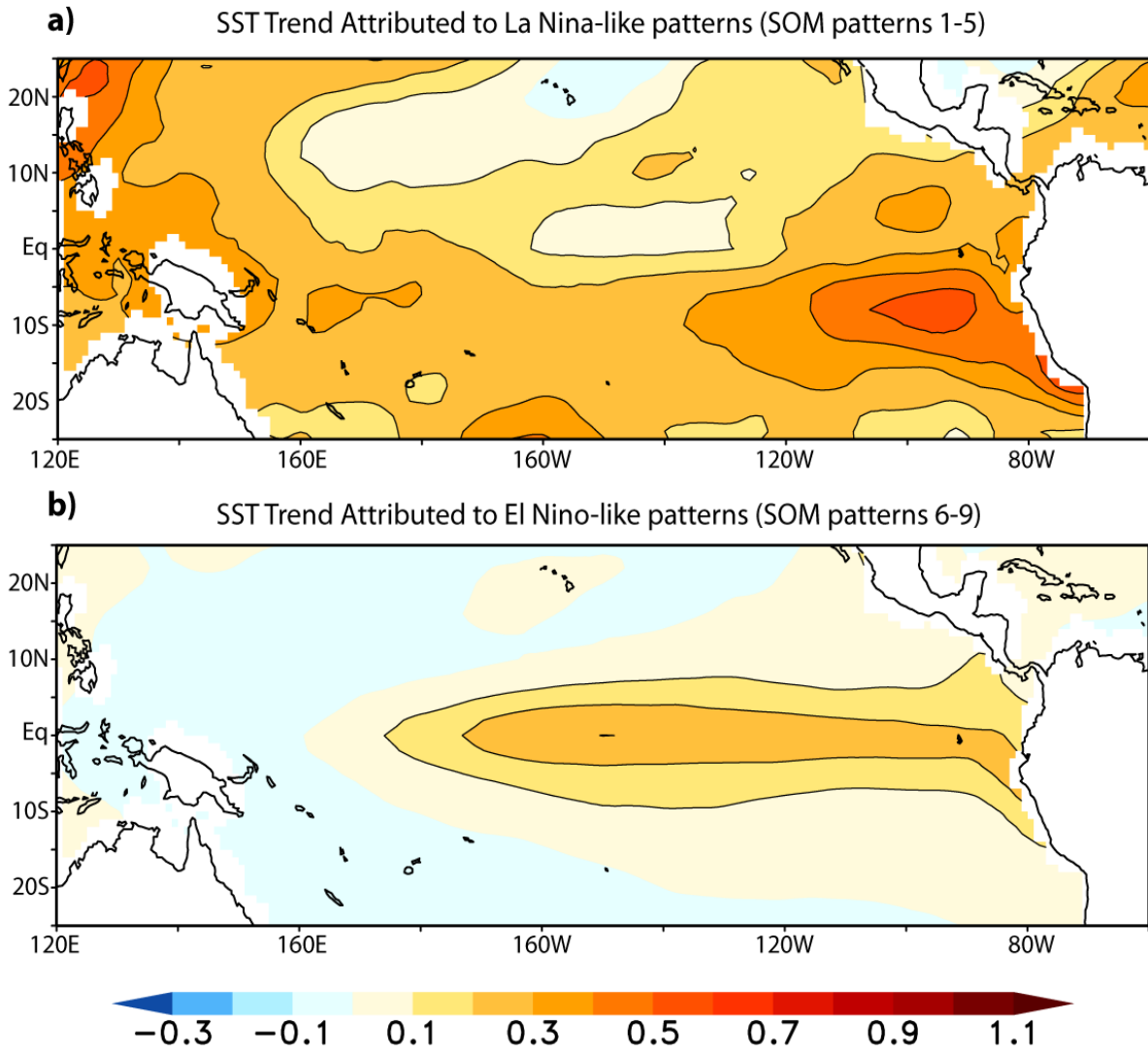b) SST Trend Attributed to El Nino-like patterns (SOM patterns 6-9)

FIG. 6. As in Fig. 5b but calculated only for (a) La Niña-like SOM patterns 1-5 and for (b) El Niño-like SOM patterns 6-9.

741